Cable lengths calculation, modelling and identification of parameters on a manipulator inspired by bird necks

Benjamin Fasquelle

Cable lengths calculation, modeling and identification of parameters on a manipulator inspired by bird necks

Benjamin Fasquelle
Ecole Centrale de Nantes,
Laboratoire des Sciences du Numérique de Nantes (LS2N)
UMR CNRS 6004, 1 rue de la Noë, 44321 Nantes
France
Email: Benjamin.Fasquelle@ls2n.fr

February 11, 2021

Contents

1 Introduction

Here we will detail the modifications to be made to the cable length calculation when taking into account the pulleys.

The application of forces on the manipulator is linked to the cables and the taking into account of the pulleys therefore modifies it.

Models of friction and elasticity of the cables will then be presented. The associated parameters will be identified in order to obtain a dynamic model allowing a good estimation of the behavior of our prototype.

2 Manipulator

We first introduce the different notations that will be useful to us later on:

- N: the number of mechanisms composing the manipulator. The mechanisms are numbered from bottom to top: the mechanism at the base of the manipulator is the first mechanism, the one just above the second mechanism, and so on until the highest mechanism which is the mechanism N.
- α: the vector of orientations. The orientation of the mechanism i is noted α_i.
- ϕ and ψ: the vectors of the orientations of the diagonal bars with respect to the base bar of each mechanism. The i elements of these vectors are noted ϕ_i and ψ_i.
- r: the radius of the pulleys. It is assumed that all pulleys have the same radius.
- L: length of the diagonal bars (identical for each mechanism)
- b: length of base bars (identical for each mechanism)
- $l(j)$ is the length of the cable associated with the motor j. The length of the cable is decomposed as follows: $l(j) = l_0(j) + \sum_{i=1}^{N} l_i(j)$, where $l_i(j)$ is the length of the part of the cable j that depends only on the mechanism i (of its geometry and orientation), and $l_0(j)$ is a constant corresponding to the rest of the cable.

In this report, we are interested in the manipulator represented in Figure (1). This one is composed of $N = 3$ mechanisms and is operated using $N_m = 4$ cables.

3 Application of forces on the manipulator

The equation of motion of the manipulator is [2]:

$$\mathbf{M}(\alpha)\ddot{\alpha} + \mathbf{c}(\alpha, \dot{\alpha}) + \mathbf{g}(\alpha) = \mathbf{Q} \tag{1}$$

where $\mathbf{M}$ is the inertia matrix, $\mathbf{c}$ the vector of Coriolis and centrifugal forces, $\mathbf{g}$ the vector of forces deriving from potential energy (gravity, spring forces) and $\mathbf{Q}$ the vector of generalized forces.

The virtual work of the force f_j applied on a wire cable j is the product of the force and the displacement of the wire cable:

$$\delta W = f_j \delta l(j) \tag{2}$$

Thus, the vector $\mathbf{Q}$ can be written as $\mathbf{Q} = \mathbf{Z}(\alpha)\mathbf{f}$ where $\mathbf{Z}$ is a matrix of size $N \times N_m$ whose elements are:

$$Z(i, j) = -\frac{\partial l_i(j)}{\partial \alpha_i} \tag{3}$$

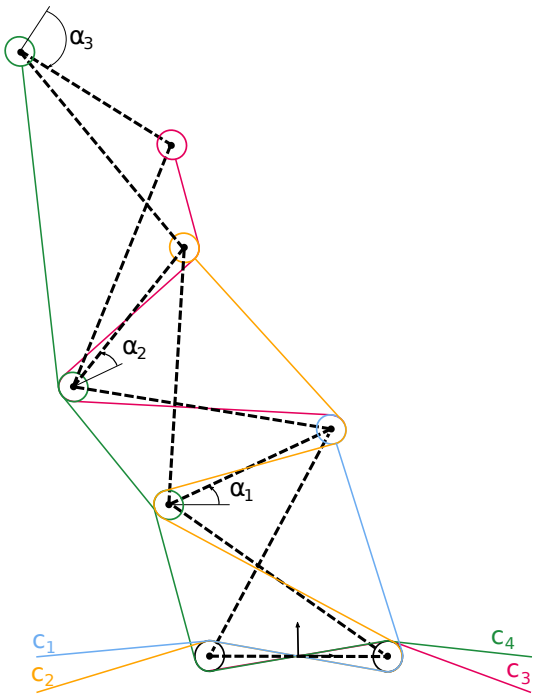

Figure 1: Wiring of the manipulator being studied.

4 Cable length

4.1 Cable extensions without pulleys

If we consider that there are no pulleys, the cables are arranged:

- either along a strut-routed bar, and the corresponding partial length is therefore that of the bar
- either on the side of a mechanism, like springs.

It is therefore necessary to calculate the lengths of the springs to the left and right of the mechanisms.

Let $d(\alpha_i)$ be the distance between the middle of the bottom bar and the middle of the top bar of mechanism i. We have:

$$d(\alpha_i) = \sqrt{L^2 - b^2 \cos^2(\frac{\alpha_i}{2})} \tag{4}$$

Let $l_l(\alpha_i)$ and $l_r(\alpha_i)$ be the lengths of the springs respectively on the left and on the right.We have:

$$l_l(\alpha_i) = d(\alpha_i) - b\sin(\frac{\alpha_i}{2}) \tag{5}$$

$$l_r(\alpha_i) = d(\alpha_i) + b\sin(\frac{\alpha_i}{2}) \tag{6}$$

The unwound lengths of the cables of our manipulator are therefore (starting from the bottom of the manipulator):

$$l_c(1) = l_r(\alpha_1) \tag{7}$$

$$l_c(2) = L + b + l_r(\alpha_2) \tag{8}$$

$$l_c(3) = 2L + 2b + l_r(\alpha_3) \tag{9}$$

$$l_c(4) = l_l(\alpha_1) + l_l(\alpha_2) + l_l(\alpha_3) \tag{10}$$

Thus, the matrix $\mathbf{Z}$ can be written in the following form:

$$\mathbf{Z} = (\mathbf{Z}_1 \;\; \mathbf{Z}_2) \tag{11}$$

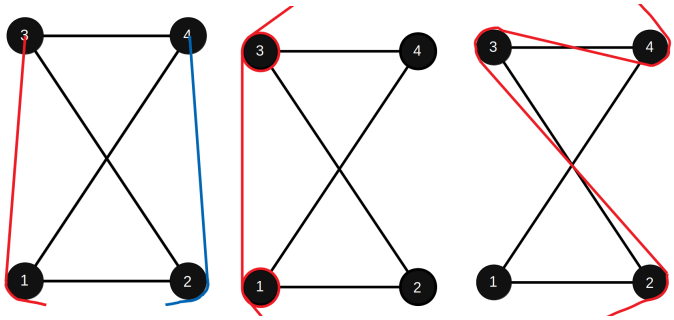

Figure 2: The different cabling studied.

where $\mathbf{Z}_1$ is a diagonal matrix:

$$\mathbf{Z}_1 = \begin{pmatrix} \frac{\partial l_r(\alpha_1)}{\partial \alpha_1} & 0 & 0 \\ 0 & \frac{\partial l_r(\alpha_2)}{\partial \alpha_2} & 0 \\ 0 & 0 & \frac{\partial l_r(\alpha_3)}{\partial \alpha_3} \end{pmatrix} \tag{12}$$

and $\mathbf{Z}_2$ a vector:

$$\mathbf{Z}_2 = \begin{pmatrix} \frac{\partial l_l(\alpha_1)}{\partial \alpha_1} \\ \frac{\partial l_l(\alpha_2)}{\partial \alpha_2} \\ \frac{\partial l_l(\alpha_3)}{\partial \alpha_3} \end{pmatrix} \tag{13}$$

4.2 Taking into account the pulleys

Decomposition

We will calculate the partial lengths of the cables passing through the mechanism i. The total length will therefore be the sum of these partial lengths.

We will study four different cases:

- The one where the cable passes on the left side of the mechanism i and is attached to the middle of the top pulley.
- The one where the cable passes on the right side of the mechanism i and is attached to the middle of the top pulley.
- The one where the cable passes on the left side of the mechanism and is wound on the top pulley to be redirected above.
- The one where the cable is strut-routed to operate upper mechanisms.

The four cases are summarized in Figure (2).

In order to delimit the portions of cables corresponding to each pulley, the lowest point of the pulley that crosses the vertical when the manipulator is in a straight position ($\alpha = 0deg$ for each mechanism) will be taken as a reference point on the pulleys. The portion of cable corresponding to a mechanism goes from this reference point of the pulley through which this cable arrives to the attachment point if the cable stops at this mechanism, or to the reference point of the exit pulley if the cable also passes through higher mechanisms. Note that when the mechanism is oriented at an angle α, the reference point on the exit pulley is moved at the same angle with respect to the vertical.

First case

The side actuated part is summarized in Figure 2 (left mechanism). The red cable pulls on the left side, is attached in the middle of the pulley 3 and wraps around the pulley 1. Symmetrically, the blue cable pulls on the right side, is attached to the middle of the pulley 4 and wraps around the pulley 2.

The partial length of this cable that depends only on this mechanism i can be written as follows:

$$l^{c1}(\alpha_i) = l_l^t(\alpha_i) + r\beta_1^1(\alpha_i) \tag{14}$$

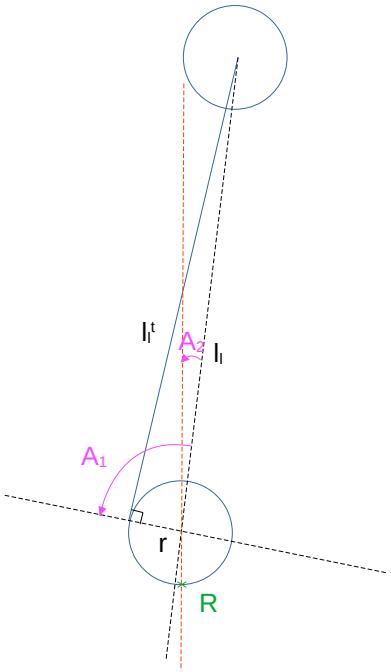

Figure 3: Actuation of a mechanism on the side: lengths and angles useful for the calculation. The red line represents the vertical axis. The blue line corresponds to the portion of cable between the middle of the upper pulley and its point of detachment from the lower pulley. The R point is taken as the reference point as the cable end point, and depends only on the lower mechanisms. The winding angle of the cable on the pulley is therefore $-A_1 + A_2 + \pi$.

where $l_l^t(\alpha_i)$ is the length of the cable between the center of the pulley 3 and the place where the cable contacts the pulley 1, and $\beta_1^1(\alpha_i)$ is the angle of winding of the cable on the pulley 1 from the reference point. The Figure (3) shows the lengths and angles useful for this calculation.

The length $l_l^t(\alpha_i)$ is obtained with the Pythagorean theorem (from the right angle shown in the Figure (3)):

$$l_l^t(\alpha_i) = \sqrt{l_l(\alpha_i)^2 - r^2} \tag{15}$$

This right angle is also used to calculate the angle A_1:

$$A_1 = atan(\frac{\sqrt{l_l(\alpha_i)^2 - r^2}}{r}) \tag{16}$$

The angle A_2 is the opposite of half of the orientation α_i of the mechanism:

$$A_2 = -\frac{\alpha_i}{2} \tag{17}$$

The angle $\beta_1^1(\alpha_i)$ is therefore:

$$\beta_1^1(\alpha_i) = \pi - atan(\frac{\sqrt{l_l(\alpha_i)^2 - r^2}}{r}) - \frac{\alpha_i}{2} \tag{18}$$

The equation (14) can therefore be rewritten:

$$l^{c1}(\alpha_i) = \sqrt{l_l(\alpha_i)^2 - r^2} + r(\pi - atan(\frac{\sqrt{l_l(\alpha_i)^2 - r^2}}{r}) \tag{19}$$

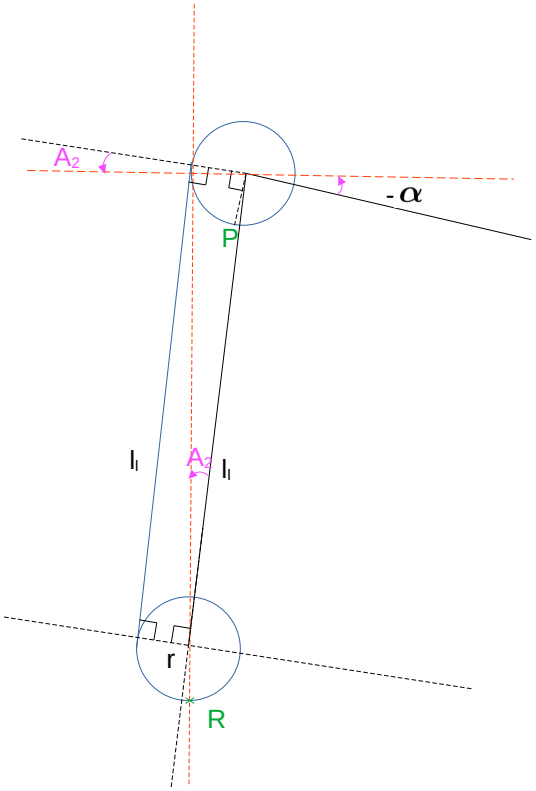

Figure 4: Actuation of a mechanism (third case): lengths and angles useful for the calculation. The red line represents the vertical axis. The blue line corresponds to the portion of cable between the detachment point on the lower pulley and the attachment point on the upper pulley. It is the same length as the black line connecting the centers of the two pulleys, because these two segments and the right angles formed with the tangent radii of the pulleys form a rectangle. The R point is taken as the reference point as the point of arrival of the cable, and depends only on the lower mechanisms. The winding angle of the cable on the lower pulley is therefore $(-\frac{\pi}{2}+A_2+\pi)$. The winding angle on the upper pulley is $(-\frac{\pi}{2}-\alpha+\pi-A_2)$.

Second case

The second case is the symmetrical of the first one (on the right side instead of the left side). With the same reasoning, the partial length of the cable is therefore:

$$l^{c2}(\alpha_i) = l_r^t(\alpha_i) + r(\pi + \frac{\alpha_i}{2} - atan(\frac{\sqrt{l_r(\alpha_i)^2 - r^2}}{r}) \tag{20}$$

with

$$l_r^t(\alpha_i) = \sqrt{l_r(\alpha_i)^2 - r^2} \tag{21}$$

Third case

The wiring studied is that of the mechanism in the middle of Figure 2. The cable is wrapped around pulley 1 and then around pulley 3, linking the two from the outside.

The portion of cable that connects the 1 and 3 pulleys is $l_l(\alpha_i)$ (see Figure (4)). So we have:

$$l^{c3}(\alpha_i) = l_l(\alpha_i) + r(\beta_1^3(\alpha_i) + \beta_3^3(\alpha_i)) \tag{22}$$

where $\beta_k^3(\alpha_i)$ is the winding angle of the cable around the pulley k which depends only on the orientation of the mechanism i.

According to the Figure (4), we have:

$$\beta_1^3(i) = \frac{\pi}{2} - \frac{\alpha_i}{2} \tag{23}$$

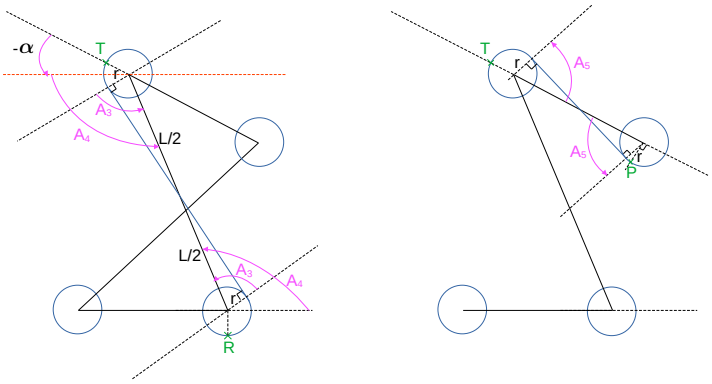

Figure 5: Actuation of a mechanism (fourth case): lengths and angles useful for the calculation. The notations are spread over two drawings to avoid overloading and to facilitate comprehension. The red line represents the horizontal axis. The blue line corresponds to the portion of cable between the detachment point on one pulley and the attachment point on the next pulley (either on the left or on the right). Whether the cable length along the diagonal bar or along the horizontal bar, the same method as in the previous cases is used to calculate their length, which is constant. The point R is taken as the reference point as the end point of the cable. The point T is a point through which the cable passes and which allows to make the junction between the two designs. The point P is taken as reference for the point where the cable exits. The winding angle of the cable on the lower pulley is $(\frac{\pi}{2}+A_4-A_3)$. The angle of the cable on the upper left pulley to the T point is $(-\alpha+A_4-A_3)$ (left figure). The angle of winding on the same pulley from the point T is $(-A_5+\pi)$ (right figure). Finally, the winding angle of the cable on the upper right pulley is $(-A_5+\frac{\pi}{2})$.

According to the same figure, the winding angle on the upper pulley is:

$$\beta_3^3(i) = \frac{3\pi}{2} - \frac{\alpha_i}{2} \tag{24}$$

We deduce that:

$$l^{c3} = l_l(\alpha_i) + r(2\pi - \alpha_i) \tag{25}$$

Fourth case

The strut-routed part is summarized in Figure 5. The cable passes through the right side of pulley 2, winds from the left side on pulley 3 and then winds from the bottom of the pulley 4.

First of all, it can be geometrically demonstrated that the portions of cables that link the pulleys have a constant length (calculable with the Pythagorean theorem). The length linking the lower right and upper left pulleys is thus $2\sqrt{(\frac{L}{2})^2-r^2}$, and the length linking the upper pulleys is $2\sqrt{(\frac{b}{2})^2-r^2}$.

So we can write:

$$l^{c4}(\alpha_i) = 2\sqrt{(\frac{L}{2})^2-r^2} + 2\sqrt{(\frac{b}{2})^2-r^2} + r(\beta_2^2(\alpha_i)+\beta_3^2(\alpha_i)+\beta_4^2(\alpha_i)) \tag{26}$$

where $\beta_k^2(\alpha_i)$ is the winding angle of the cable around the pulley k which depends only on the orientation of the mechanism i.

The angles represented on the Figure (5) are $A_3 = atan(\frac{L}{2r}), A_4 = \psi_i, A_5 = atan(\frac{b}{2r})$.

So we have:

$$\beta_2^2(i) = \frac{\pi}{2} + \psi_i - atan(\frac{L}{2r}) \tag{27}$$

$$\beta_3^2(i) = -\alpha_i + \psi_i - atan(\frac{L}{2r}) - atan(\frac{b}{2r}) + \pi \tag{28}$$

$$\beta_4^2(i) = -atan(\frac{b}{2r}) + \frac{\pi}{2} \tag{29}$$

We can therefore deduce that:

$$\begin{aligned} l^{c4}(\alpha_i) =& 2\sqrt{(\frac{L}{2})^2 - r^2} + 2\sqrt{(\frac{b}{2})^2 - r^2} \\ &+ r\Big(\frac{\pi}{2} + \psi_i - atan(\frac{L}{2r}) - \alpha_i + \psi_i - atan(\frac{L}{2r}) - atan(\frac{b}{2r}) + \pi - atan(\frac{b}{2r}) + \frac{\pi}{2}\Big) \end{aligned} \tag{30}$$

This result happens to be symmetrical in α. This implies that the symmetric strut-routed case has the same relative cable length.

Synthesis

The unwound lengths of the cables of our manipulator are therefore (starting from the bottom of the manipulator):

$$l_c(1) = l^{c2}(\alpha_1) \tag{31}$$

$$l_c(2) = l^{c4}(\alpha_1) + l^{c2}(\alpha_2) \tag{32}$$

$$l_c(3) = l^{c4}(\alpha_1) + l^{c4}(\alpha_2) + l^{c2}(\alpha_3) \tag{33}$$

$$l_c(4) = l^{c3}(\alpha_1) + l^{c3}(\alpha_2) + l^{c1}(\alpha_3) \tag{34}$$

Thus, the matrix $\mathbf{Z}$ can be written in the following form:

$$\mathbf{Z} = (\mathbf{Z}_1 \;\; \mathbf{Z}_2) \tag{35}$$

where $\mathbf{Z}_1$ is a triangular matrix:

$$\mathbf{Z}_1 = \begin{pmatrix} \frac{\partial l^{c2}(\alpha_1)}{\partial \alpha_1} & \frac{\partial l^{c4}(\alpha_1)}{\partial \alpha_1} & \frac{\partial l^{c4}(\alpha_1)}{\partial \alpha_1} \\ 0 & \frac{\partial l^{c2}(\alpha_2)}{\partial \alpha_2} & \frac{\partial l^{c4}(\alpha_2)}{\partial \alpha_2} \\ 0 & 0 & \frac{\partial l^{c2}(\alpha_3)}{\partial \alpha_3} \end{pmatrix} \tag{36}$$

and $\mathbf{Z}_2$ a vector:

$$\mathbf{Z}_2 = \begin{pmatrix} \frac{\partial l^{c3}(\alpha_1)}{\partial \alpha_1} \\ \frac{\partial l^{c3}(\alpha_2)}{\partial \alpha_2} \\ \frac{\partial l^{c1}(\alpha_3)}{\partial \alpha_3} \end{pmatrix} \tag{37}$$

5 Dynamic model

We now present the dynamic model of our system. First, we will present a basic dynamic model, assuming that the cables are rigid. Then, we will present the dynamic model including the elasticity of the cables and the motor friction.

5.1 Basic dynamic model

Assuming that the cables are rigid and neglecting friction, a first dynamic model can be written as follows [2]:

$$\mathbf{M}(\alpha)\ddot{\alpha} + \mathbf{c}(\alpha, \dot{\alpha}) + \mathbf{g}(\alpha) = \mathbf{Z}(\alpha)\mathbf{f} \tag{38}$$

where $\mathbf{g}$ is the vector of forces deriving from a potential energy (gravity, spring forces), $\mathbf{f} = [f_1, f_2, f_3, f_4]^T$ is the vector of the forces applied by the motors and transmitted by the cables, $\mathbf{M}$ is the matrix of intertia taking into account the inertia of the manipulator $\mathbf{M}_m$ [1] and the inertia of the motors:

$$\mathbf{M}(\alpha) = \mathbf{M}_m(\alpha) + I_a(\frac{R}{r_d})^2\mathbf{Z}(\alpha)^T \tag{39}$$

where I_a is the inertia of the motors. $\mathbf{c}$ is the vector of Coriolis effects, defined by $\mathbf{c}_m$ and the effects of the motors:

$$\mathbf{c} = \mathbf{c}_m(\alpha) + I_a(\frac{R}{r_d})^2 \dot{\mathbf{Z}}(\alpha, \dot{\alpha})\mathbf{Z}(\alpha)^T \tag{40}$$

The control law tested in [2] was based on this dynamic model, but large oscillations in the applied forces were observable and the values of α calculated for the control were different from the observable values. In order to have a better control, an improved dynamic model is proposed below, including the motor friction and the elasticity of the ropes.

No attempt will be made to identify the parameters of the above dynamic model. Indeed, all data is available from the CAD model of our prototype and the manufacturer's motor data sheets. In order to have high available forces $\mathbf{f}$, a high reduction ratio is used in the motor gearboxes ($R = 25$). Moreover, since tensegrity systems are inherently light, the contribution of the manipulator inertia is negligible compared to that of the gearmotors. On the other hand, we note that the latter is taken into account via the $\mathbf{Z}$ matrix, which depends on the cable routing and α. The inertia matrix $\mathbf{M}$ is therefore variable and it is important to take this into account in our models and in the order.

5.2 Dynamic model with friction and cable elasticity

All cables are now considered elastic. Assuming that $\theta_i = 0,\ i = 1,...,4$ when the manipulator is in $\alpha_i = 0, i = 1,...3$ at rest (i.e. with zero applied forces and, therefore, with zero cable elongations), the vector of elastic cable elongations $\mathbf{x}_c = [x_{c1}, x_{c2}, x_{c3}, x_{c4}]^T$ is defined as:

$$\mathbf{x}_c = \mathbf{l}_c - \mathbf{l}_{c0} - \frac{r_d}{R}\theta \tag{41}$$

In other words, the elongation of each cable is defined as the difference between its theoretical length as calculated in section 4.2 and the length of cable wrapped around the associated winch.

Differentiating Eq. (41) with respect to time gives :

$$\mathbf{Z}(\alpha)^T \dot{\alpha} = \frac{r_d}{R}\dot{\theta} + \dot{\mathbf{x}}_c \tag{42}$$

Let $\mathbf{t}_c = [t_{c1}, t_{c2}, t_{c3}, t_{c4}]^T$ be the vector of cable tensions and $\mathbf{f}_{friction}$ be the vector of friction forces. Most friction occurs in motor gearboxes. Modeling friction in pulleys can be interesting to improve the accuracy of cable force transducer measurements [5]. In this article, no cable force transducers are used. Therefore, we focus on the friction coming from motor gearboxes. The dynamic model written for the system composed of motor gearboxes and cables provides the equation of motion of θ :

$$I_a\ddot{\theta} + \frac{r_d}{R}\mathbf{t}_c + \frac{r_d}{R}\mathbf{f}_{friction} = \frac{r_d}{R}\mathbf{f} \tag{43}$$

The dynamic model written for the manipulator and the cables gives the equation of motion of α :

$$\mathbf{M}_m(\alpha)\ddot{\alpha} + \mathbf{c}_m(\alpha, \dot{\alpha}) + \mathbf{g}(\alpha) = \mathbf{Z}(\alpha)\mathbf{t}_c \tag{44}$$

By differentiating the equation (42) with respect to time and substituting $\ddot{\theta}$ for the equation (43), the tension in the cables can be expressed as follows :

$$\mathbf{t}_c = \mathbf{f} - \mathbf{f}_{friction} - I_a(\frac{R}{r_d})^2(\mathbf{Z}(\alpha)^T\ddot{\alpha} + \dot{\mathbf{Z}}(\alpha, \dot{\alpha})^T\dot{\alpha} - \ddot{\mathbf{x}}_c) \tag{45}$$

Substituting the above expression in Eq (44) gives the dynamic model of the complete system with the friction and elasticity of the cable :

$$\mathbf{M}(\alpha)\ddot{\alpha} + \mathbf{c}(\alpha, \dot{\alpha}) + \mathbf{g}(\alpha) = \mathbf{Z}(\alpha)\left(\mathbf{f} - \mathbf{f}_{friction} + I_a(\frac{R}{r_d})^2\ddot{\mathbf{x}}_c\right) \tag{46}$$

Now it is necessary to identify the friction and elasticity of the cables.

6 Identification

6.1 Friction formulas

As we have written previously, it is assumed that friction occurs mainly in geared motors. A modeled dry friction can be written as follows:

$$\mathbf{f}_{dry}(\mathbf{f}_s, \dot{\theta}) = diag(sign(\dot{\theta}))\mathbf{f}_s \tag{47}$$

where $\mathbf{f}_s = [f_s(1), f_s(2), f_s(3), f_s(4)]^T$ is a constant vector that must be identified, $diag(\mathbf{v})$ is a diagonal matrix of size (4×4) constructed with the components of $\mathbf{v}$ and *sign* is the sign function. A model ensuring continuity can be derived as follows:

$$\mathbf{f}_{dry}(\mathbf{f}_s, \dot{\theta}) = diag(\frac{2}{\pi} atan(c_m \dot{\theta}))\mathbf{f}_s \tag{48}$$

where c_m is a setting parameter that adjusts the slope of the arc tangent around 0. This parameter is arbitrarily set to $c_m = 0.5$. The factor $\frac{2}{\pi}$ ensures that $\mathbf{f}_{friction}$ tends towards $\mathbf{f}_s$ and $-\mathbf{f}_s$ when $\dot{\theta}$ has positive and negative values, respectively.

Viscous friction can be modeled as follows:

$$\mathbf{f}_{visc}(\mathbf{f}_v, \dot{\theta}) = diag(\dot{\theta})\mathbf{f}_v \tag{49}$$

where $\mathbf{f}_v = [f_v(1), f_v(2), f_v(3), f_v(4)]^T$ is a constant vector that must be identified.

Thus, the friction of the engines are:

$$\mathbf{f}_{friction}(\mathbf{f}_s, \mathbf{f}_v, \dot{\theta}) = \mathbf{f}_{dry}(\mathbf{f}_s, \dot{\theta}) + \mathbf{f}_{visc}(\mathbf{f}_v, \dot{\theta}) \tag{50}$$

Substituting $\mathbf{f}_{friction}$ for Eq (46), we get :

$$\mathbf{Z}(\alpha)(diag(\frac{2}{\pi} atan(c_m \dot{\theta}))\mathbf{f}_s + diag(\dot{\theta})\mathbf{f}_v) = \mathbf{Z}(\alpha)(\mathbf{f} + I_a(\frac{R}{r_d})^2 \ddot{\mathbf{x}}_c) - \mathbf{M}(\alpha)\ddot{\alpha} - \mathbf{c}(\alpha, \dot{\alpha}) - \mathbf{g}(\alpha) \tag{51}$$

We thus obtain a system of three equations that are linear in $\mathbf{f}_s$ and $\mathbf{f}_v$. Once α, θ, their derivatives and $\mathbf{f}$ are known, we can identify $\mathbf{f}_s$ and $\mathbf{f}_v$.

6.2 Cable elasticity formulas

During the identification experiments, α is obtained from the image processing and θ is measured by the engine encoders. The cable elongation $\mathbf{x}_c$ can be calculated with Eq. (41), namely

$$\mathbf{x}_c = \mathbf{l}_c(\alpha) - \mathbf{l}_{c0} - \frac{r_d}{R}\theta \tag{52}$$

This calculation assumes that there is no cable elongation in the initial configuration of the right-hand manipulator. In practice, the cables must be slightly stretched to prevent slackening, but the resulting elongation is small and can be neglected. The $\dot{\mathbf{x}}_c$ derivative of $\mathbf{x}_c$ is calculated numerically.

We will study three models of cable stiffness. The first is a general cable model that allows us to identify a set of parameters for each cable:

$$\mathbf{t}_{ci} = k(i)x_{ci} + c_a(i)\dot{x}_{ci} \tag{53}$$

or, as a vector :

$$\mathbf{t}_c = diag(\mathbf{x}_c)\mathbf{k} + diag(\dot{\mathbf{x}}_c)\mathbf{c}_a \tag{54}$$

where $\mathbf{k} = [k(1), k(2), k(3), k(4)]^T$ is the constant vector of cable stiffnesses and $\mathbf{c}_a = [c_a(1), c_a(2), c_a(3), c_a(4)]^T$ is the constant vector of damping coefficients. Using the equation (43) and the friction model, the tension in the cable can be written :

$$\mathbf{t}_c = \mathbf{f} - \mathbf{f}_{friction} - \frac{R}{r_d} I_a \ddot{\theta} \tag{55}$$

Combination of eqs. (54) and (55), we obtain the following vector equation :

$$diag(\mathbf{x}_c)\mathbf{k} + diag(\dot{\mathbf{x}}_c)\mathbf{c}_a = \mathbf{f} - \mathbf{f}_{friction} - \frac{R}{r_d} I_a \ddot{\theta} \tag{56}$$

This vector equation provides four equations that are linear in the coefficients of friction, stiffness and damping of each cable.

The second and third elastic models are based on the Young's modulus [4]:

$$\mathbf{t}_c = diag(\mathbf{x}_c)\frac{ES}{\mathbf{l}} + diag(\dot{\mathbf{x}}_c)\frac{cS}{\mathbf{l}} \tag{57}$$

where S is the section of the cable. E is Young's modulus and c is a damping coefficient, both to be identified. $\mathbf{l}$ is the length of the cable: for the second model we will take $\mathbf{l} = \mathbf{l}_0$ the total length of the cable, while in the third model we will take $\mathbf{l} = \mathbf{l}_c$ the unwound length of the cable.

Using the same method as in the first model, we obtain:

$$diag(\mathbf{x}_c)\frac{ES}{\mathbf{l}} + diag(\dot{\mathbf{x}}_c)\frac{cS}{\mathbf{l}} = \mathbf{f} - \mathbf{f}_{friction} - \frac{R}{r_d}I_a\ddot{\theta} \tag{58}$$

This vector equation also provides four equations that are linear in the coefficients of friction, stiffness and damping for each cable.

6.3 Full identification model

The equations (51) and (56), which describe the contribution of friction in the dynamic model and the stiffness model of the cables, respectively, are now assembled to obtain a system of linear equations with the parameters to be identified :

$$\mathbf{D}\mathbf{v} = \mathbf{y} \tag{59}$$

where $\mathbf{v}$ is the vector of $n_p = 12$ parameters to be identified $\mathbf{v} = \begin{pmatrix}\mathbf{k} & \mathbf{c}_a & \mathbf{f}_s\end{pmatrix}^T$. Now, the contribution of friction in Eqs. (51) and (56) are not of the same order because the coefficients of $\mathbf{Z}$ are of the order of 10^{-2}. To avoid any discrepancy, Eq (56) is multiplied by a weight $W = 100$.

The vector $\mathbf{y}$ is given by:

$$\mathbf{y} = \begin{pmatrix} \mathbf{f} - \frac{R}{r_d}I_a\ddot{\theta} \\ \\ W(\mathbf{Z}(\mathbf{f} + I_a(\frac{R}{r_d})^2\ddot{\mathbf{x}}_c) - \mathbf{M}\ddot{\alpha} - \mathbf{g} - \mathbf{c}) \end{pmatrix} \tag{60}$$

and $\mathbf{D}$ is written:

$$\mathbf{D} = \begin{pmatrix} diag(\mathbf{x}_c) & diag(\dot{\mathbf{x}}_c) & diag(\frac{2}{\pi}atan(c_m\dot{\theta}))\ \mathbf{0}_{3\times 4} & \mathbf{0}_{3\times 4} & W\mathbf{Z}diag(\frac{2}{\pi}atan(c_m\dot{\theta})) \end{pmatrix} \tag{61}$$

Friction parameters are also independently identified for comparison with the overall identification. In this case, there are only parameters $n_p = 8$ to be identified, $\mathbf{v} = [\mathbf{f}_s \quad \mathbf{f}_v]^T$ and :

$$\mathbf{y} = \mathbf{f} - \frac{R}{r_d}I_a\ddot{\theta} \tag{62}$$

$$\mathbf{D} = [diag(\frac{2}{\pi}atan(c_m\dot{\theta}))\ \ diag(\dot{\theta})]. \tag{63}$$

6.4 Method of identification

Motive forces $\mathbf{f}$ and positions θ and orientation angles α are sampled along a specific trajectory to obtain r sampled values. Then, $\mathbf{v}$ can be estimated as the least square solution $\hat{\mathbf{v}}$ of the linear system :

$$\mathbf{W}\mathbf{v} + \rho = \mathbf{Y} \tag{64}$$

where $\mathbf{W}$ is an observation matrix $(r \times n_p)$ defined by sampling the regressor $\mathbf{D}$ defined in (61) or (63), $\mathbf{Y}$ is a sampling of $\mathbf{y}$ defined in (60) or (62), ρ is the vector of residuals or the vector of errors. The number r of samples must be greater than the number of parameters to be identified: $r > n_p$ [3].

The vector parameter $\mathbf{v}$ minimizing the standard 2 of ρ is given by :

$$\mathbf{v} = \mathbf{W}^+\mathbf{Y} \tag{65}$$

	Dry friction	Viscous friction
$f_s(1)(N)$	12.91	4.68×10^{-2}
relative σ_i	5.62%	56.85%
$f_s(2)(N)$	16.72	4.63×10^{-2}
relative σ_i	4.55%	72.11%
$f_s(3)(N)$	18.11	4.64×10^{-2}
relative σ_i	4.25%	83.42%
$f_s(4)(N)$	16.09	0.72×10^{-2}
relative σ_i	1.85%	105.96%

	Dry friction only
$f_s(1)(N)$	14.13
relative σ_i	2.52%
$f_s(2)(N)$	17.70
relative σ_i	2.02%
$f_s(3)(N)$	18.97
relative σ_i	1.88%
$f_s(4)(N)$	16.29
relative σ_i	1.25%

Table 1: Identified friction parameters. The viscous parameters are badly identified.

The quality of the solution depends on the $\mathbf{W}$ conditioning, which depends on the choice of the trajectory made during the identification process. If the measurement noises are independent in W and Y, the quality of the identification can be evaluated with the covariance matrix $\mathbf{C}_X$:

$$\mathbf{C}_X = \sigma_\rho^2 (\mathbf{W}^T \mathbf{W})^{-1} \tag{66}$$

where $\sigma_\rho^2 = \frac{||\mathbf{Y}-\mathbf{W}\mathbf{v}||^2}{r-N_p}$. The standard deviation of parameter i is $\sigma_i = \sqrt{\mathbf{C}_X(i,i)}$ and the confidence interval is given by $2\sigma_i$. The relative standard deviation 100 $\frac{\sigma_i}{\mathbf{v}_i}$ evaluates the quality of the identification of the parameter i.

6.5 Filtering

The data used for identification are the measurements of the angular position of the motor θ, the input actuating forces $\mathbf{f}$ (assuming perfect electrical response of the motors) and the manipulator configuration α evaluated from the image processing. Cable elongations are deduced from (41), after initialization in straight position. The derivatives of the measured quantities are calculated by centered numerical differentiation after filtering.

It is essential to filter the measured data to avoid biases resulting from discrete and noisy measurements (41). A Butterworth low-pass filter is used to filter forward and backward measurements with the Matlab function *filtfilt*. The derivatives of θ are obtained with a central difference algorithm to avoid phase shift. The cutoff frequency of the Butterworth filter is calculated with the method explained in [6].

The video frequency used to measure the orientation of the mechanisms is $30Hz$, while the frequency of the control law is $500Hz$. To synchronize the data, the motor encoder measurements are resampled with the Matlab *decimate* procedure at $31.25Hz$, the value closest to $30Hz$. The video data is also resampled to $31.25Hz$ with linear interpolation.

6.6 Results

6.6.1 Identification of dry and viscous friction

At first, only friction is identified, and in two different ways:

- On the one hand, dry and viscous friction is identified.
- On the other hand, only dry friction is identified, neglecting viscous friction.

The identified parameters are in the Table 1. Dry friction is well identified in both cases, but viscous friction is not: its relative standard deviation is well above 10%.

The Figure (6) shows the plots of the $\mathbf{Z}(\alpha)\mathbf{f}$ couples from the forces and their reconstruction with the equation (51), with and without the friction model, and with and without the viscous friction. The objective is to highlight the contribution of friction terms and to show that these terms must be taken into account. However, it shows that viscous friction, in addition to being poorly identified, does not allow for a better estimation of couples. For this reason, we will only consider dry friction in the rest of this report.

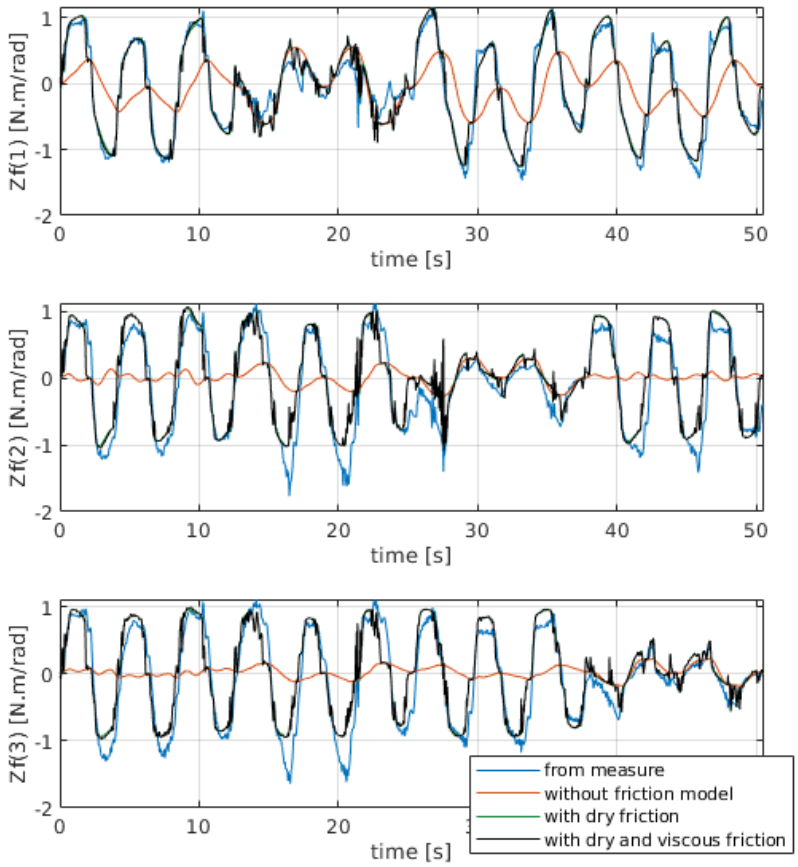

Figure 6: Plots of $\mathbf{Z}(\alpha)\mathbf{f}$ with the dynamic model, including friction or not, and from measurement data. Torques evaluated with friction model are clearly closer to the measured ones. The viscous friction does not modify a lot the curve in comparision with the sole dry friction.

6.6.2 Identification of cable elasticity

Here, the dry friction and elasticity of the cables are identified, with the three elastic models offered.

The identified parameters are in the Table 2. The dry friction is well identified and similar whatever the elastic model. Stiffness parameters are well identified in all three models, but damping parameters are poorly identified in all three cases. This is due to the low values of the elongation rate.

There are two ways to calculate the tension in cables: by the applied forces and friction on the one hand, and by the elastic model and elongation on the other hand. The Figure (7) shows the tension in the cables. calculated by the forces applied and the friction identified (taking those identified in the previous section, all values identified here being strongly similar), and the tension calculated by the elastic models identified. It is shown that the three elastic models have different results but none of them can faithfully reproduce the tension calculated by the forces. The mean error of reconstruction is $6.88N$ for Model 1, $9.84N$ for Model 2 and $9.64N$ for Model 3.

The Figure (8) shows the reconstruction error of each model as a function of the tension calculated by the applied forces. It shows that for each model and each cable, the error increases as the tension increases. Non-linear cable models should therefore be more suitable.

	Model 1	Model 2	Model 3
$\boldsymbol{f}_s(1)(N)$	14.42	14.38	14.32
relative σ	1.68%	1.73%	1.72%
$\boldsymbol{f}_s(2)(N)$	17.65	17.49	17.48
relative σ	1.38%	1.44%	1.42%
$\boldsymbol{f}_s(3)(N)$	18.77	18.41	18.48
relative σ	1.32%	1.38%	1.35%
$\boldsymbol{f}_s(4)(N)$	16.18	16.32	16.29
relative σ	0.88%	0.90%	0.89%
$\boldsymbol{k}(1)$ $(N.m^{-1})$	10454	-	-
relative σ	1.37%	-	-
$\boldsymbol{k}(2)$ $(N.m^{-1})$	9256	-	-
relative σ	1.60%	-	-
$\boldsymbol{k}(3)$ $(N.m^{-1})$	8319	-	-
relative σ	1.85%	-	-
$\boldsymbol{k}(4)$ $(N.m^{-1})$	5336	-	-
relative σ	1.28%	-	-
E (GPa)	-	4.04	1.23
relative σ	-	0.83%	0.81%
$\boldsymbol{c}_a(1)$ $(N.s.m^{-1})$	805	-	-
relative σ	30.5%	-	-
$\boldsymbol{c}_a(2)$ $(N.s.m^{-1})$	333	-	-
relative σ	68.7%	-	-
$\boldsymbol{c}_a(3)$ $(N.s.m^{-1})$	-218	-	-
relative σ	94.3%	-	-
$\boldsymbol{c}_a(4)$ $(N.s.m^{-1})$	370	-	-
relative σ	64.3%	-	-
c $(MPa.s^{-1})$	-	139.8	57.4
relative σ	-	45.5%	32.88%

Table 2: Identified stiffness and damping parameters for three mechanisms.

7 Conclusion

In this report, we have first detailed the calculations of the cable lengths, which are used in the dynamic model. These calculations are detailed without and with consideration of the pulleys, which have an impact on the shape of the matrix **Z**. Indeed, in comparison with the calculation without pulleys, the pulleys modify the non-zero values of **Z** and add some, corresponding to the strut-routed passage of the cables.

We then presented a dynamic model and added a friction model and an elasticity model of the cables.

In order to exploit these new models, the friction parameters were identified. The dry frictions are well identified and allow a better estimation of the forces by the dynamic model. Viscous friction is poorly identified and does not improve the model, so it is neglected.

Three elastic cables models were then compared, identifying the parameters specific to each one. For each model, the stiffness coefficients are well identified while the damping coefficients are not. All three models show interesting results, but they are less good when the tension in the cabes is high. Non-linear elastic models could therefore be more efficient.

References

[1] Fasquelle Benjamin et al. “Dynamic modeling and control of a tensegrity manipulator mimicking a bird neck”. In: *Advances in Mechanism and Machine Science, IFToMM WC 2019*. Ed. by Tadeusz Uhl. Vol. 73. Cham: Springer, 2019, pp. 2087–2097. DOI: 10.1007/978-3-030-20131-9_207.

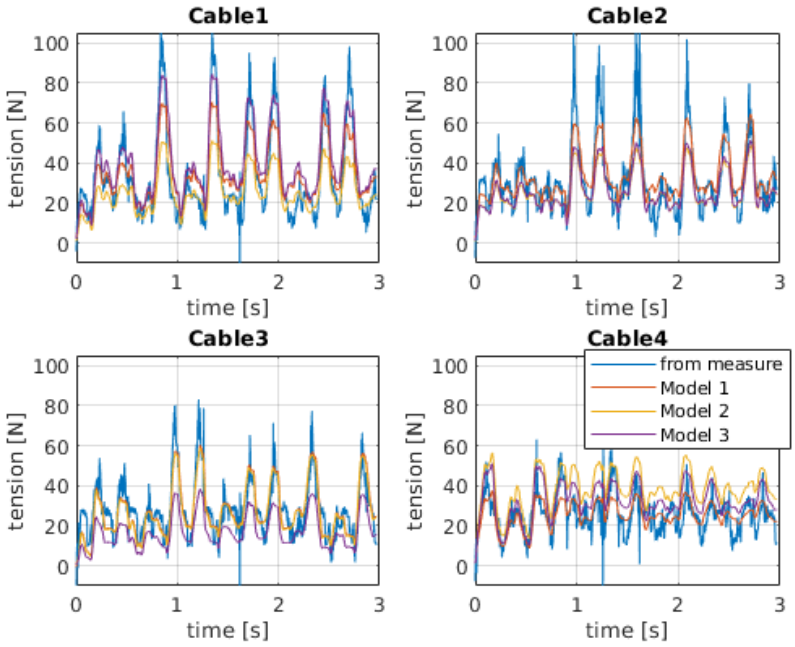

Figure 7: Tension in the cables, calculated by forces and elastic models.

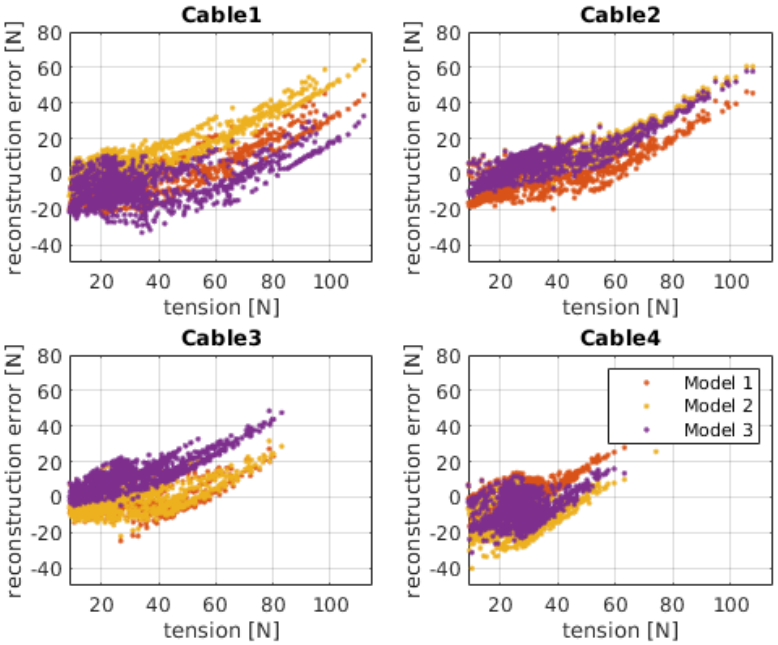

Figure 8: Error in reconstructing the tension in the cables, according to the tension calculated by the applied forces.

[2] Benjamin Fasquelle et al. “A bio-inspired 3-DOF light-weight manipulator with tensegrity X-joints”. In: *ICRA’2020*. 2020.

[3] Wisama Khalil and Etienne Dombre. *Modeling, identification and control of robots*. Butterworth-Heinemann, 2004.

[4] Mohammad A Khosravi and Hamid D Taghirad. “Dynamic analysis and control of fully-constrained cable robots with elastic cables: variable stiffness formulation”. In: *Cable-Driven Parallel Robots*. Springer, 2015, pp. 161–177.

[5] W. Kraus, M. Kessler, and A. Pott. “Pulley friction compensation for winch-integrated cable force measurement and verification on a cable-driven parallel robot”. In: *2015 IEEE International Conference on Robotics and Automation (ICRA)*. 2015, pp. 1627–1632. DOI: 10.1109/ICRA.2015.7139406.

[6] Minh Tu Pham, Maxime Gautier, and Philippe Poignet. “Identification of joint stiffness with bandpass filtering”. In: *Proceedings 2001 ICRA. IEEE International Conference on Robotics and Automation (Cat. No. 01CH37164)*. Vol. 3. IEEE. 2001, pp. 2867–2872.